Dimensionality Control of Vapochromic Hydrogen-Bonded Proton-Transfer Assemblies Composed of a Bis(hydrazone)iron(II) Complex
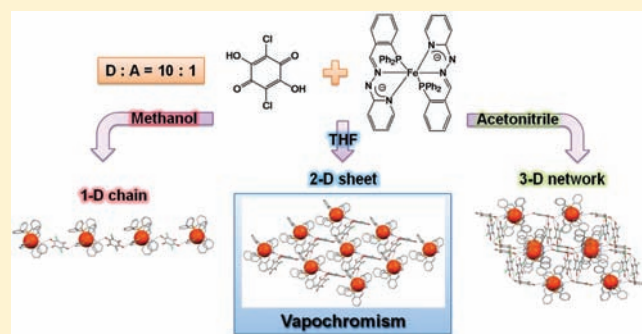
Mee Chang,[†] Atsushi Kobayashi,*,[†] Kiyohiko Nakajima,[‡] Ho-Chol Chang,[†] and Masako Kato*,[†]

[†]Department of Chemistry, Faculty of Science, Hokkaido University, North-10 West-8, Kita-ku, Sapporo 060-0810, Japan
[‡]Department of Chemistry, Aichi University of Education, Igaya, Kariya, Aichi 448-8542, Japan

S *Supporting Information*

ABSTRACT: We describe the novel synthesis of a bis-(hydrazone)iron(II) complex in protonated $[Fe(Hpbph)_2]Cl_2$ (**1**) and deprotonated $[Fe(pbph)_2]$ (**2**) forms and several hydrogen-bonded proton-transfer (HBPT) assemblies having different dimensionalities of hydrogen-bonded network structures, $[Fe(Hpbph)_2]$ $(CA)\cdot 2CH_3OH$ (**3**), $[Fe(Hpbph)_2](HCA)_2\cdot 2THF$ (**4**), and $[Fe(Hpbph)_2](CA)(H_2CA)_2\cdot 2CH_3CN$ (**5**) (Hpbph = 2-(diphenylphosphino)benzaldehyde-2-pyridylhydrazone), consisting of a deprotonated Fe(II)–hydrazone complex (**2**) as a proton acceptor (A) and chloranilic acid (H_2CA) as a proton donor (D). The deprotonated complex **2** exhibited two-step reversible protonation reactions to form the double-protonated form **1**, and the acid-dissociation constants were determined to be 7.6 and 10.3 in methanol solution. Utilizing this proton-accepting ability of **2**, we succeeded in synthesizing HBPT assemblies **3**, **4**, and **5** from the reactions in CH_3OH, THF, and CH_3CN, respectively, with the same D/A ratio of $H_2CA/[Fe(pbph)_2]$ = 10:1. These assemblies were found to have one-dimensional (1-D), two-dimensional (2-D), and three-dimensional (3-D) hydrogen-bonded networks with D/A ratios of 1:1, 2:1, and 3:1 for **3**, **4**, and **5**, respectively. In **3**, a 1-D hydrogen-bonded chain composed of the alternate arrangement of $[Fe(Hpbph)_2]^{2+}$ and CA^{2-}, $\{\cdots[Fe(Hpbph)_2]^{2+}\cdots CA^{2-}\cdots\}_\infty$, was surrounded by solvated methanol molecules to form isolated 1-D hydrogen-bonded chains. In the HBPT assembly **4**, a 2-D hydrogen-bonded sheet was formed from two types of hydrogen-bonded chains, $\{\cdots[Fe(Hpbph)_2]^{2+}\cdots HCA^-\cdots HCA^-\cdots\}_\infty$ and $\{\cdots HCA^-\cdots HCA^-\cdots\}_\infty$, and solvated THF molecules did not form any hydrogen bonds. In **5**, two orthogonal hydrogen-bonded chains constructed from the neutral chloranilic acid molecules, $\{\cdots CA^{2-}\cdots 2(H_2CA)\cdots\}_\infty$, were formed in addition to the 1-D hydrogen-bonded chain similar to that in **3**, resulting in the formation of a rigid 3-D hydrogen-bonded network structure. By controlling the dimensionality of the hydrogen bond network, we found that the 2-D HBPT assembly **4** is sufficiently flexible to exhibit interesting vapochromic behavior in response to various organic vapors.

INTRODUCTION

Vapochromic materials, which show dramatic and reversible color changes upon exposure to vapors of volatile organic compounds, have attracted much attention in terms of their potential application as chemical sensors.[1–10] Remarkable vapochromism has been observed in various transition-metal assemblies from the adsorption and desorption of organic vapors, leading to significant variations in metal–metal interactions,[11–15] solvent–metal bonds,[16] conformation of ligands,[17] and stacking interactions between complexes.[12,18] Among these, metal–metal interactions have attracted increasing attention for their vapor-sensing applications and can lead to interesting properties, such as reversible vapochromic luminescence of stacking homometallic Pt–Pt[11,12] and Au–Au[13] and heterometallic Au–Ag[14] and Au–Cu[15] complexes. These complexes exhibit vapochromic behavior in response to reversible rearrangements by solvent vapor or interstitial solvation

of volatile organic compounds.[19] In such molecular assembling systems, there remain challenges in successfully achieving vapor recognition and/or selective sensing functions, probably because of the difficulty of controlling the crystal structure, including intermolecular interactions.

Hydrogen-bonded proton transfer (HBPT) plays an important role in physical, chemical, and biological processes.[20] The hydrogen-bonded self-assembly of molecular components in supramolecular architectures has provided interesting multidimensional systems with unique frameworks and potentially useful properties in separation, catalysis, and sensor technology.[21] In such a hydrogen-bonded self-assembled system, anilic acids (3,6-substituted-2,5-dihydroxy-1,4-benzoquinones, H_2XA,

Table 1. Crystal Parameters and Refinement Data

				complex		
	Hpbph	1	2	3	4	5
formula	$C_{24}H_{20}N_3P$	$C_{52}H_{56}N_6O_4Cl_2FeP_2$	$C_{48}H_{44}N_6O_3FeP_2$	$C_{56}H_{48}N_6O_6Cl_2FeP_2$	$C_{68}H_{58}N_6O_{10}Cl_4FeP_2$	$C_{70}H_{50}N_8O_{12}Cl_6FeP_2$
formula weight	381.42	1017.70	870.71	1089.73	1378.85	1525.67
crystal system	monoclinic	monoclinic	monoclinic	monoclinic	monoclinic	monoclinic
space group	$P2_1/n$	$C2/c$	$P2_1/n$	$P2_1/n$	$C2$	$C2/c$
a/Å	8.021(11)	20.769(19)	12.063(19)	12.990(6)	20.193(5)	20.708(4)
b/Å	11.259(16)	12.245(7)	17.409(3)	17.096(7)	12.370(3)	12.233(3)
c/Å	22.046(3)	19.218(16)	19.406(4)	22.592(9)	13.889(3)	26.914(6)
α/°	90	90	90	90	90	90
β/°	99.400(8)	92.300(4)	91.544(7)	105.730 (3)	115.091 (10)	102.174(10)
γ/°	90	90	90	90	90	90
V/Å^3	1946.1(5)	4883.3(7)	4073.7(12)	4829.0(3)	3141.9(13)	6665(2)
Z	4	4	4	4	2	4
T/K	150(1)	150(2)	150(1)	150(1)	150(1)	150(2)
D_{cal}/g·cm^{-3}	1.290	1.384	1.413	1.499	1.457	1.521
reflections collected	15415	19170	31691	37988	12971	27064
unique reflections	4491	5560	9307	11046	6224	7632
GOF	1.040	1.042	1.061	1.087	1.049	1.095
R	0.0383	0.0321	0.0461	0.0884	0.0413	0.0838
R_W	0.1028	0.0933	0.1191	0.2299	0.1092	0.1922

X = H, F, Cl, Br, I, and CN) are well-known and interesting building blocks, because these compounds can work as strong diprotic acids with excellent proton-donating groups and undergo multistage deprotonation processes.[22] Among them, chloranilic acid exists in three forms, the neutral yellow H_2CA at very low pH, the purple HCA^-, which is most stable at pH 2, and the pale violet CA^{2-}, stable at high pH.[23] The charge of H_2CA can be controlled by proton-transfer ability as well as degree of solubility of the proton donor and proton acceptor in solvents.[22b] They can be associated with various proton acceptors to give new hydrogen-bonded supramolecular architectures.

Hydrogen-bonded networks, which have flexible and directional characteristics, can be transformed for the adsorption and desorption of vapor molecules. Kawata et al. reported the reversible vapochromic behavior of zigzag chains of the copper complex $\{[Cu(bhnq)(H_2O)_2]H_2O\cdot 3EtOH\}_n$ (H_2bhnq = 2,2′-bi(3-hydroxy-1,4-naphthoquinone)) based on conformational change in the ligand and hydrogen-bonded networks between the chain and solvent vapors.[24] Recently, we synthesized a series of metal—hydrazone complexes using different metal ions and found that the coordination geometry of the metal center plays an important role in their acid—base behavior.[25] Using the controllable acid—base property of the metal—hydrazone complex as a hydrogen-bonding module, we reported a vapochromic material, $\{[PdBr(Hmtbhp)]_2(HBA)_2(H_2BA)\cdot 2CH_3CN\}$ (Hmtbhp = 2-(2-(2-(methylthio)benzylidene)hydrazinyl)pyridine), composed of a Pd(II)—hydrazone complex as a proton acceptor and bromanilic acid (H_2BA) as a proton donor.[26] This assembly exhibits interesting vapochromic behavior in response to the proton-donating ability of the vapor molecule, and this recognition ability is believed to be strongly related to the manner of hydrogen bonding.

In the present work, in order to improve this vapor recognition ability and clarify the role of the hydrogen-bonded network in the vapochromic response, we have extended our research to focus on the dimensionality control of the hydrogen bonding. To develop a multidimensional HBPT system and clarify the vapochromic behavior, we first synthesized new bis(hydrazone)iron(II) complexes $[Fe(Hpbph)_2]Cl_2$ (**1**) and $[Fe(pbph)_2]$ (**2**) (Hpbph = 2-(diphenylphosphino)benzaldehyde-2-pyridylhydrazone), because these octahedral complexes would have two hydrogen-bonding sites in opposite directions, which lead to the formation of an infinite one-dimensional (1-D) hydrogen-bonded chain structure. Taking advantage of this feature of the bis(hydrazone)iron(II) complex, we newly synthesized three types of HBPT assemblies, $\{[Fe(Hpbph)_2](CA)\cdot 2CH_3OH\}$ (**3**), $\{[Fe(Hpbph)_2](HCA)_2\cdot 2THF\}$ (**4**), and $\{[Fe(Hpbph)_2](CA)(H_2CA)_2\cdot 2CH_3CN\}$ (**5**) (H_2CA = chloranilic acid), by using **2** as a proton acceptor and chloranilic acid as a proton donor. In the present paper, we report the syntheses, X-ray structures, and characterization of bis(hydrazone)Fe(II) complexes and their HBPT assemblies and demonstrate that the HBPT assembly **4** with a 2-D hydrogen-bonded network is sufficiently flexible to exhibit interesting vapochromic behavior in the presence of various organic solvent vapors ranging from relatively low-polar to highly polar vapors.

■ EXPERIMENTAL SECTION

General Procedures. All commercially available starting materials were used as received, and solvents were used without any purification. Unless otherwise stated, all manipulations were performed in air. $FeCl_3\cdot 6H_2O$ and H_2CA were purchased from Wako Pure Chemical Industries Ltd., Japan. The hydrazone ligand (Hpbph) was prepared according to the published method.[27]

$\{[Fe(Hpbph)_2]Cl_2\cdot 4CH_3OH\}$ (**1**). To $FeCl_3\cdot 6H_2O$ (36 mg, 0.13 mmol) in methanol (10 mL) was added solid Hpbph (101 mg, 0.27 mmol). The mixture was stirred for 30 min at room temperature. After natural evaporation of the solvent for a few days, red crystals emerged. The crystals were isolated by filtration and washed using a small amount of methanol. Yield: 90 mg, 76%. Elemental analysis calculated for $C_{52}H_{56}Cl_2N_6O_4P_2Fe$: C, 61.37;

Table 2. Selected Bond Lengths and Angles of the Free Ligand Hpbph, Fe(II)−Hydrazone Complexes 1 and 2, and HBPT Assemblies 3, 4, and 5

	Hpbph	1	2	3	4	5
N1−C5	1.337(16)	1.347(2)	1.361(2)	1.340(6)	1.331(3)	1.342(6)
(N4−C29)			1.365(2)	1.352(6)		
C5−N2	1.385(17)	1.356(19)	1.339(2)	1.367(6)	1.350(4)	1.366(6)
(C29−N5)			1.341(2)	1.352(6)		
N2−N3	1.361(15)	1.382(17)	1.387(2)	1.389(4)	1.385(3)	1.374(5)
(N5−N6)			1.392(2)	1.373(5)		
N3−C6	1.280(16)	1.306(18)	1.314(2)	1.295(6)	1.300(4)	1.305(6)
(N6−C30)			1.305(2)	1.305(6)		
C6−C7	1.469(15)	1.451(2)	1.450(2)	1.463(5)	1.459(4)	1.452(6)
(C30−C31)			1.454(2)	1.445(7)		
C5−N2−N3	118.54(11)	118.15(13)	112.35(16)	117.3(4)	117.3(2)	117.9(4)
(C29−N5−N6)			112.26(16)	118.1(4)		
N1−Fe−N3		82.08(5)	80.85(6)	82.30(15)	82.18(10)	82.41(16)
(N4−Fe−N6)			80.95(7)	82.09(17)		

H, 5.55; N, 8.26. Found: C, 61.37; H, 5.55; N, 8.29. ^{1}H NMR (dmso-d_6): δ 14.03 (s, 1H, −NH), 9.52 (s, 1H), 7.86 (d, 1H), 7.44 (s, 1H), 7.27−6.81 (m, 12H), 6.55 (s, 3H), 6.36 (d, $J = 7.5$ Hz, 1H).

{[Fe(pbph)$_2$]·3H$_2$O} (**2**). To **1** (52 mg, 0.05 mmol) in acetonitrile (10 mL) was added an excess amount of triethylamine. The mixture was stirred for 30 min at room temperature, and dark red crystals were filtered. The product was washed with diethyl ether. Yield: 43 mg, 97%. Elemental analysis calculated for C$_{48}$H$_{44}$N$_6$O$_3$P$_2$Fe: C, 66.21; H, 5.09; N, 9.65. Found: C, 66.51; H, 5.00; N, 9.70. ^{1}H NMR (dmso-d_6): δ 9.16 (s, 1H, −CH═), 7.61 (d, $J = 6.2$ Hz, 1H), 7.52 (t, $J = 7.9$ Hz, 1H), 7.09−6.97 (m, 6H), 6.85−6.74 (m, 5H), 6.69−6.55 (m, 3H), 5.85 (d, $J = 9.1$ Hz, 1H), 5.78 (t, $J = 6.2$ Hz, 1H).

{[Fe(Hpbph)$_2$](CA·2CH$_3$OH} (**3**). To **2** (10 mg, 0.01 mmol) in methanol (20 mL) was added a methanol solution of H$_2$CA (25 mg, 0.12 mmol). The mixture was stirred for 1 h at room temperature. Red crystals formed after a few days of natural evaporation. The crystals were isolated by filtration and washed with a small amount of methanol. Yield: 11 mg, 88%. Elemental analysis calculated for C$_{56}$H$_{48}$Cl$_2$N$_6$O$_6$P$_2$Fe: C, 61.72; H, 4.44; N, 7.71. Found: C, 60.92; H, 4.43; N, 7.73.

{[Fe(Hpbph)$_2$](HCA)·2THF} (**4**). Complex **4** was obtained through a synthetic method similar to that used to obtain **3**, but using THF instead of methanol. Brick-red crystals formed after a few days. Yield: 14 mg, 89%. Elemental analysis calculated for C$_{68}$H$_{58}$Cl$_4$N$_6$O$_{10}$P$_2$Fe: C, 59.23; H, 4.24; N, 6.10. Found: C, 59.32; H, 4.44; N, 6.01.

{[Fe(Hpbph)$_2$](CA)(H$_2$CA)$_2$·2CH$_3$CN} (**5**). Complex **5** was obtained through a synthetic method similar to that used to obtain **3**, but using acetonitrile instead of methanol. Red crystals formed after a few days. Yield: 14 mg, 80%. Elemental analysis calculated for C$_{70}$H$_{50}$Cl$_6$N$_8$O$_{12}$P$_2$Fe: C, 55.11; H, 3.30; N, 7.34. Found: C, 55.13; H, 3.39; N, 7.22.

Single-Crystal X-ray Diffraction Measurements. All single-crystal X-ray diffraction measurements were performed using a Rigaku Mercury charge-coupled device diffractometer with graphite monochromated Mo Kα radiation ($\lambda = 0.71069$ Å) and a rotating anode generator. Each single crystal was mounted on a glass fiber with epoxy resin. The crystal temperature was cooled using a N$_2$-flow-type temperature controller. Diffraction data were collected and processed using CrystalClear software.[28] Structures were resolved by a direct method using SIR-92 for Hpbph and **2**−**4**, and SHELXS-97 for **1** and **5**.[29,30] Structural refinements were performed via full-matrix least-squares using SHELXL-97. The non-hydrogen atoms were refined anisotropically, and hydrogen atoms were refined using the riding model. The crystallographic data are summarized in Table 1.
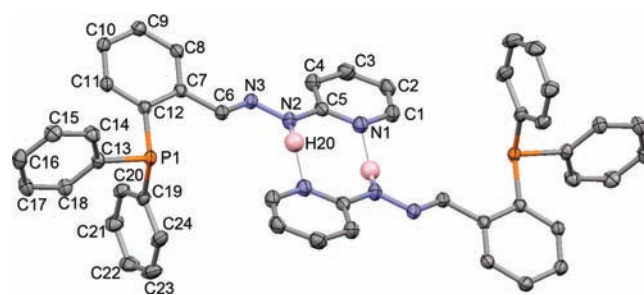
Figure 1. Dimerized structure of the Hpbph ligand with thermal ellipsoids drawn at the 50% probability level. Carbon-bound hydrogen atoms are omitted for clarity.

UV−vis Spectroscopy. The UV−vis absorption spectrum of each complex was recorded on a Shimadzu UV-2400PC spectrophotometer. The diffuse reflectance spectrum of each complex was recorded on the same spectrophotometer equipped with an integrating-sphere apparatus. Obtained reflectance spectra were converted to absorption spectra using the Kubelka−Munk function $F(R_\infty)$.

IR Spectroscopy. IR spectra were recorded with a JASCO 4100 FT-IR spectrometer. Temperature-dependent IR spectra were recorded on a Thermo-Nicolet 6700 FT-IR spectrometer using a Nicolet Continuum microscope. The sample temperature was controlled by a Linkam LK-600 hotstage.

Thermogravimetric Analysis. Thermogravimetry (TG) and differential thermal analysis were performed using a Rigaku ThermoEvo TG8120 analyzer.

Powder X-ray Diffraction. Powder X-ray diffraction was conducted using a Rigaku SPD diffractometer at beamline BL-8B at the Photon Factory, KEK, Japan. The wavelength of the synchrotron X-rays was 1.200(1) Å. All samples were placed in a glass capillary with a diameter of 0.5 mm.

■ RESULTS AND DISCUSSION

Crystal Structures of Hydrazone Ligand and Bis-(hydrazone)iron(II) Complexes. *Hpbph.* The ligand Hpbph was synthesized using a Schiff base condensation reaction with 2-(diphenylphosphino)benzaldehyde and 2-hydrazinopyridine, as reported previously.[27] The ligand crystallized in the monoclinic
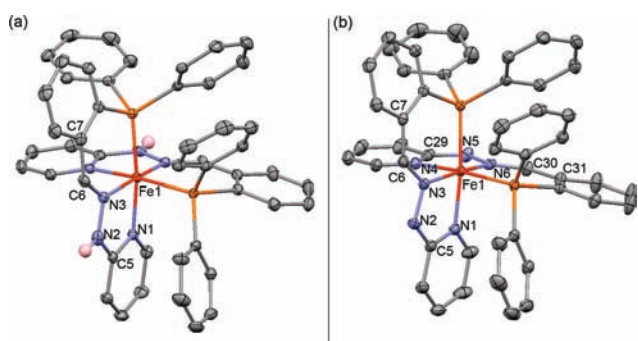
Figure 2. Molecular structures of (a) the protonated **1** and (b) deprotonated **2** forms with thermal ellipsoids drawn at the 50% probability level. Carbon-bound hydrogen atoms are omitted for clarity.

space group $P2_1/n$. Selected bond lengths and angles are presented in Table 2. The dimerized structure of Hpbph ligands through double hydrogen bonds is shown in Figure 1. The pyridyl ring and benzyl ring are twisted and linked by a zigzag −NH−N=CH− spacer in a transoid conformation. Molecules of Hpbph were dimerized by intermolecular double hydrogen bonds between the pyridyl nitrogen (N1) and the imine nitrogen (N2−H) in the adjacent ligand (3.076(17) Å).

*Protonated Form {[Fe(Hpbph)$_2$]Cl$_2$·4CH$_3$OH} (**1**).* The protonated form **1** was obtained by the reaction of Fe(III) chloride with the Hpbph ligand in methanol. It should be noted that the obtained complex was also characterized by ^{1}H NMR spectroscopy, suggesting that the paramagnetic Fe(III) ion was reduced in this reaction to form the low-spin diamagnetic Fe(II) complex. The molecular structure of **1** is shown in Figure 2a. The complex **1** crystallized in the monoclinic space group $C2/c$, with one [Fe(Hpbph)$_2$]$^{2+}$ cation, two Cl$^-$ counteranions, and four methanol molecules. Two Hpbph ligands are crystallographically equivalent. The geometry of **1** around the Fe(II) ion is an octahedron occupied by four nitrogen atoms (N1, N3, N1′, and N3′) and two phosphorus atoms (P1 and P1′) from the two Hpbph ligands. The coordination of the ligand to the Fe(II) ion caused the −NH−N=CH− linkage to rotate at both ends from transoid to cisoid conformation and affected the bond lengths of Hpbph.[31] As shown in Table 2, the C5−N2 distance significantly decreased by about 0.03 Å, whereas those of N2−N3 and N3−N6 increased by about 0.02 and 0.03 Å upon coordination with the Fe(II) ion. In the crystal structure of **1**, intermolecular hydrogen bonds are present between the imine nitrogen and neighboring chloride anion and between the chloride anion and two methanol molecules.

*Deprotonated Form {[Fe(pbph)$_2$]·3H$_2$O} (**2**).* Upon mixing **1** and triethylamine in acetonitrile, the deprotonated form **2** was obtained. Conversion between the protonated **1** and deprotonated **2** occurred reversibly in the methanol solution by the addition of 2 equiv of perchloric acid or triethylamine (see below). The complex **2** was also characterized by ^{1}H NMR spectroscopy, suggesting that the Fe(II) center is in the low-spin diamagnetic state. The molecular structure of **2** is shown in Figure 2b. Complex **2** crystallized in the monoclinic space group $P2_1/n$ with one neutral [Fe(pbph)$_2$] complex and three water molecules. As with **1**, the Fe(II) ion of **2** has distorted octahedral coordination geometry and is coordinated by four nitrogen atoms (N1, N3, N4, and N6) and two phosphorus atoms (P1
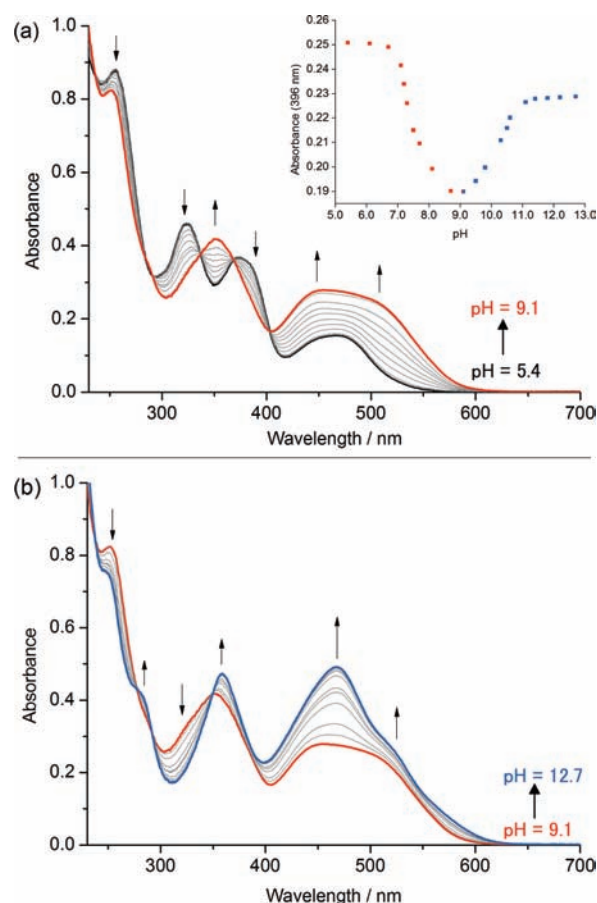

Figure 3. Absorption spectral change in **1** in methanol at room temperature at pH regions (a) between 5.4 and 9.1 and (b) between 9.1 and 12.7. The inset graph shows pH dependence of the absorbance at 396 nm.

and P2) from two pbph ligands of different environments. The Fe−N bond lengths are in the range of 1.939(15)−1.991(16) Å. The distances for high-spin Fe(III) complexes are expected to be around 2.1 Å.[32] Thus, this complex can be assigned as the Fe(II) low-spin state. In the comparison of the protonated (**1**) and deprotonated (**2**) forms, the deprotonation of the Hpbph ligand affected the rearrangement of the bond lengths on the hydrazone part. As shown in Table 2, the N1−C5 bond distance of complex **2** is longer by about 0.014 Å than that of **1**, whereas the C5−N2 is shorter by about 0.017 Å. The C5−N2−N3 and N1−Fe−N3 bond angles are also smaller by about 5.8° and 1.2°, respectively, than those of **1**. The differences suggest that the π electron on the pyridine ring is delocalized on not only the ring but also the hydrazone moiety. This structural difference between the protonated and deprotonated forms has been observed in the Pd(II)−hydrazone complex, [PdBr(mtbhp)] (Hmtbhp = 2-(2-(2-(methylthio)benzylidene)hydrazinyl)pyridine).[25] The neutral molecule of **2** also formed intermolecular hydrogen bonds with the lattice water molecules at the nitrogen in the deprotonated hydrazone moiety.

Protonation and Deprotonation Reactions of Metal−Hydrazone Complexes. As described above, some of the metal−hydrazone complexes show a reversible protonation/deprotonation reaction in the solution state. To examine the acid−base behavior of the bis(hydrazone)iron(II) complex, we

measured electronic absorption spectra at various pH conditions in methanol. As shown in Figure 3, the protonated Fe(II) complex **1** in methanol exhibited four relatively intense adsorption bands at 256, 324, 373, and 465 nm. Via titration of a methanolic potassium hydroxide solution, the absorption spectrum of the complex changed in two steps. In the first step observed in the pH range between 5.4 and 9.1, new bands at 351, 445, and 520 nm appeared gradually with the three isosbestic points at 337, 368, and 403 nm, respectively, as shown in Figure 3a. In the second step shown in Figure 3b, a new band at 358 nm appeared with an increase in the absorption band at 468 nm. According to papers published so far,[25,33] the energy of intraligand charge-transfer transition of the hydrazone ligand is known to be remarkably affected by protonation at the imine nitrogen of the hydrazone moiety through the addition of acid. Thus, the two-step spectral changes in this bis(hydrazone)iron(II) complex are also attributable to the deprotonation reaction at
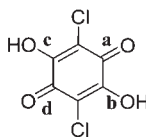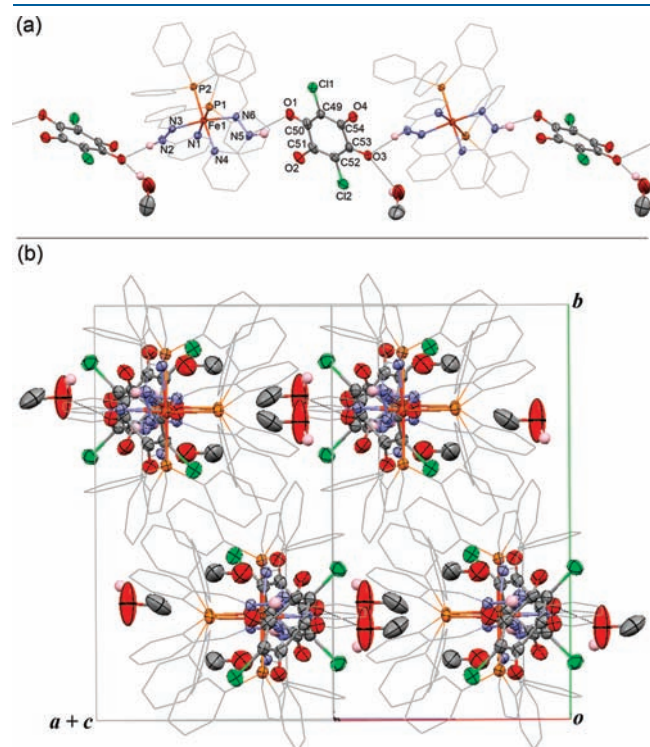

Figure 4. (a) 1-D hydrogen-bonded chain structure along the $a - c$ axis and (b) packing diagram viewed down along the $a - c$ axis of **3**. Carbon-bound hydrogen atoms are omitted and carbon atoms in the hydrazone ligand are drawn as stick models for clarity. Dotted lines represent hydrogen bonds.

the hydrazone moiety. It should be emphasized that the original spectrum of **1** was recovered completely by the addition of perchloric acid. The results indicate that deprotonation/protonation of the Fe(II)−hydrazone complex reversibly occurs by adding potassium hydroxide and perchloric acid. The inset of Figure 3a shows a plot of absorbance changes against pH at 396 nm. From the bell-shaped curve, the first (pK_{a_1}) and second (pK_{a_2}) dissociation constants were determined to be 7.6 and 10.3, respectively. The dissociation constant for the square-planar Pt(II) complex with the same Hpbph ligand [PtCl-(Hpbph)]Cl is 6.6 under the same methanol solution. Comparing the Fe(II)− and the Pt(II)−hydrazone complexes, the pK_{a_1} value of the Fe(II)−hydrazone complex is slightly larger than that of the Pt(II) complex. This may be attributed to the higher planarity of the square-planar Pt(II)−hydrazone complex and/or the trans effect of the opposite Hpbph ligand.

Crystal Structures of Hydrogen-Bonded Proton-Transfer Assemblies. With the aim of controlling the dimensionality of the hydrogen-bonded network, we synthesized three HBPT assemblies composed of deprotonated **2** as a proton acceptor (A) and chloranilic acid as a proton donor (D). The HBPT assemblies **3**, **4**, and **5** were prepared successfully in methanol, THF, and acetonitrile, respectively, with the same D/A ratio of $H_2CA/2 = 10:1$. Interestingly, despite the same reaction ratio, three different HBPT assemblies with 1-D, 2-D, and 3-D hydrogen-bonded network structures were obtained in the different solvents. In this section, we discuss the crystal structures of these HBPT assemblies, particularly the hydrogen-bonded network structure.

1:1 Assembly of [Fe(pbph)2] and H2CA. The 1:1 assembly **3** crystallized in the monoclinic space group $P2_1/n$, with one acceptor, one donor, and two methanol molecules. Figure 4a shows the hydrogen-bonded chain formed from donor and acceptor molecules. Selected bond lengths and angles around the hydrazone part and chloranilic acid are summarized in Tables 2 and 3. The bond lengths of the hydrazone part in **3** are close to those of the completely protonated complex **1**. For example, the −C−NH−N= angles of 118.1° and 117.3° around the N2 and N5 atoms, respectively, are close to those of **1** and larger than those of deprotonated nitrogen atoms (112.26° for N2 and 112.35° for N5) in complex **2**. Thus, the Fe(II)−hydrazone complex can be assigned as the completely protonated form, $[Fe(Hpbph)_2]^{2+}$. Accordingly, the donor moiety of **3** adopted a dianionic chloranilate, CA^{2-}, which is supported by the four short C−O bond distances, as shown in Table 3. Therefore, two-proton transfer from H_2CA to the deprotonated Fe(II)−hydrazone complex should occur in the reaction solution. The large difference in pK_a values between chloranilic acid ($pK_{a_1} = 1.09$ and $pK_{a_2} = 2.42$)[24(b)] and **1** also

Table 3. Selected Bond Lengths of the Chloranilic Acid in HBPT Assemblies 3, 4, and 5 Compared to Those in H_2CA, $HCA^−$, and $CA^{2−a,b,c}$

		H_2CA [a]	$HCA^−$ [b]	$CA^{2−}$ [c]	3	4	5
	a	1.222	1.233	1.243	1.237(7)	1.212(3)	1.235(6)	1.213(6)
	b	1.322	1.253	1.253	1.259(6)	1.270(4)	1.263(6)	1.317(6)
	c	1.322	1.324	1.243	1.234(6)	1.313(4)	-	1.323(6)
	d	1.222	1.222	1.253	1.254(6)	1.231(3)	-	1.216(6)

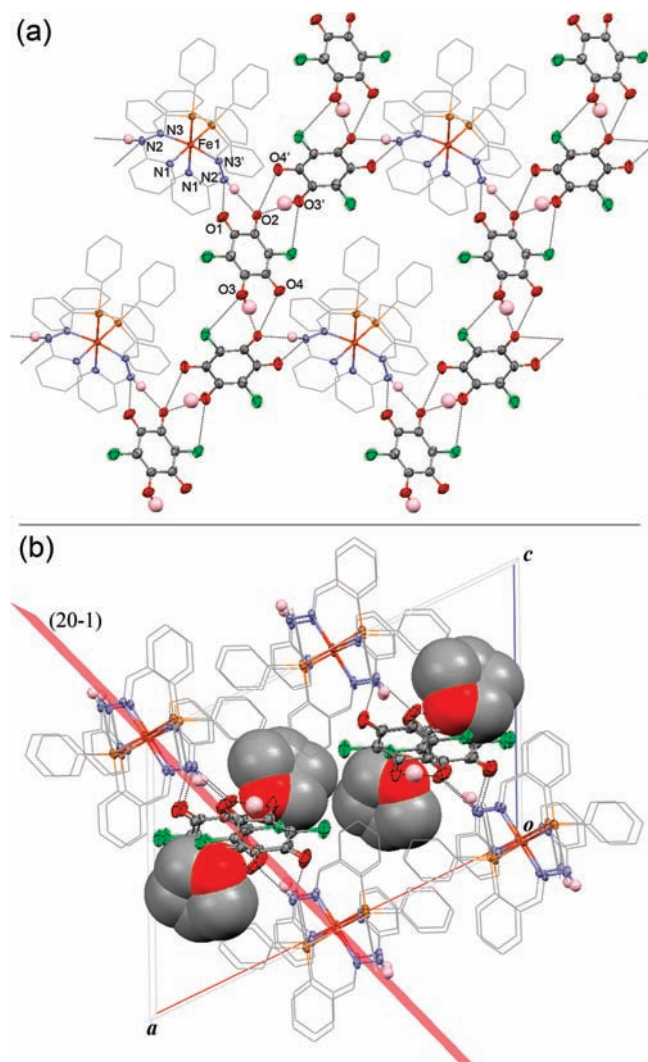[a] Reference 34. [b] Reference 35. [c] Reference 36.

Figure 5. (a) 2-D hydrogen-bonded sheet structure and (b) packing diagram of **4** viewed down along the *b* axis. Carbon-bound hydrogen atoms are omitted and carbon atoms in the hydrazone ligand are drawn as stick models for clarity. Dotted lines represent hydrogen bonds. THF molecules are shown as space-filling models. The red plane shown in (b) is the (20-1) plane.

support this result. In the crystal structure, infinite 1-D hydrogen-bonded chains along the *a − c* axis were formed from the alternate arrangement of $[Fe(Hpbph)_2]^{2+}$ and CA^{2-}, as shown in Figure 4a. The hydrogen bond distances between the N sites of $[Fe(Hpbph)_2]^{2+}$ and the O sites of chloranilate are 2.711(6) and 2.715(6) Å, respectively, which are close to the typical distance of the N−H···O-type hydrogen bond.[23(c)] It should be noted that the solvated methanol molecules were found to be hydrogen-bonded to the oxygen atom (O3) of the chloranilate with a distance of 2.793(8) Å. Thus, the hydrogen-bonded methanol acts as the terminals of the hydrogen-bonded network, as shown in Figure 4b, resulting in low dimensionality of the hydrogen bond network in this assembly.

1:2 Assembly of [Fe(pbph)₂] and H₂CA. The 1:2 assembly **4** crystallized in the monoclinic space group *C2*, with one acceptor, two donors, and two THF molecules. Figure 5a shows the hydrogen-bonded network structure of **4**. Because bond distances and angles around the hydrazone part similar to those in
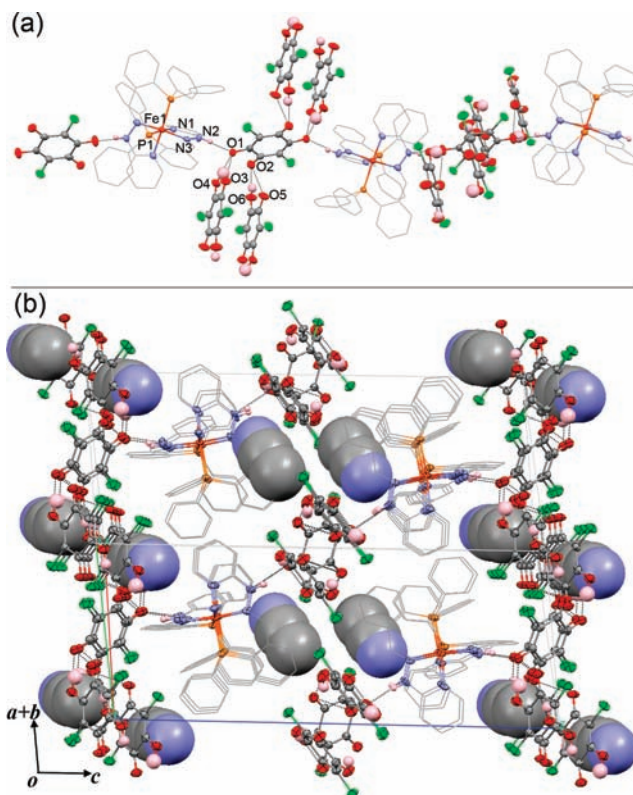

Figure 6. (a) Hydrogen-bonded chain structure with three different directions and (b) packing diagram of **5** viewed down along the *a − b* axis. Carbon-bound hydrogen atoms are omitted and carbon atoms in the hydrazone ligand are drawn as stick models for clarity. Dotted lines represent hydrogen bonds. Acetonitrile molecules are shown as space-filling models.

the protonated form **1** were observed for **4**, as shown in Table 2, the acceptor received two protons as well as the HBPT assembly **3**. In contrast, the C−O bond distances of two donor molecules clearly indicate that the molecules are assigned to monoanionic chloranilate, HCA⁻. Therefore, two protons transferred from two H₂CA molecules to the acceptor molecule. In this assembly, there are two types of 1-D hydrogen-bonded chains, as shown in Figure 5a. One is the 1-D chain formed from one acceptor and two donor molecules as $\{\cdots[Fe(Hpbph)_2]^{2+}\cdots HCA^-\cdots HCA^-\cdots\}_\infty$. The other is constructed of only the HCA⁻ anions as $\{\cdots HCA^-\cdots HCA^-\cdots\}_\infty$, which is along the *b* axis and is perpendicular to the former type of chain. According to the results, a 2-D hydrogen-bonded sheet was formed in the (20-1) plane. Solvated THF molecules are located between these two 2-D hydrogen-bonded sheets, as shown in Figure 5b, and formed no hydrogen bonds. The hydrogen bond distances between $[Fe(Hpbph)_2]^{2+}$ and HCA⁻ are 2.930(4) and 2.739(3) Å, which are close to the typical values of N−H···O hydrogen bonds.[37] The hydrogen bond distance between two HCA⁻ anions is 2.799(3) Å for O4−H···O2, which is longer by about 0.11 Å than the typical distance of the O−H···O-type hydrogen bond.[37]

1:3 Assembly of [Fe(pbph)₂] and H₂CA. The 1:3 assembly **5** crystallized in the monoclinic space group *C2/c*, with one acceptor, three donor molecules, and two acetonitrile molecules. Figure 6a shows the hydrogen-bonded network structure of **5**. The bond distances and angles in hydrazone moieties are close to
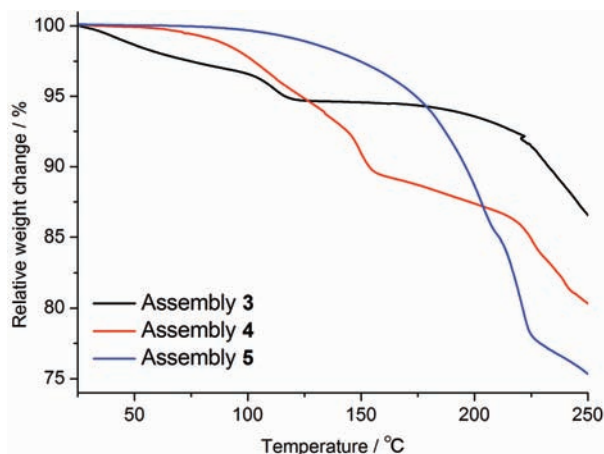
Figure 7. Thermogravimetric analysis traces for the HBPT assemblies **3−5** (5 K/min heating; Ar flow rate, 300 mL/min).

Figure 8. Changes in powder X-ray diffraction patterns of the HBPT assemblies **3** and **4** before and after removal of the solvated molecules (λ = 1.200(1) Å).

those of the protonated form **1**, as shown in Table 2. Of the three donor moieties, one with four relatively short C−O bond distances can be assigned to the dianionic chloranilate, CA^{2-}, and the other two with two longer C−O bonds above 1.3 Å are in the neutral state, H_2CA. Thus, the acceptor unit received two protons from one donor molecule to form a 1-D hydrogen-bonded chain along the $a + c$ axis as $\{\cdots[Fe(Hpbph)_2]^{2+}\cdots CA^{2-}\cdots\}_\infty$, which is similar to that in the HBPT assembly **3**, as shown in Figure 6a. Interestingly, the hydrogen bond between $[Fe(Hpbph)_2]^{2+}$ and CA^{2-} (2.644 Å) is shorter than that of assembly **3** by about 0.06 Å. No hydrogen bond was formed between the neutral chloranilic acids and the $[Fe(Hpbph)_2]^{2+}$ unit. Judging from the interplanar distance between two adjacent H_2CA molecules (ca. 3.34 Å), the $\pi-\pi$ stacking interaction is effective between them. These $\pi-\pi$ stacked neutral chloranilic acids formed two orthogonal hydrogen-bonded chains with the dianionic CA^{2-} as $\{\cdots CA^{2-}\cdots 2(H_2CA)\cdots\}_\infty$, which extended along the $a + b$ and $b - a$ axes, as shown in Figure 6a. The hydrogen bond distances between CA^{2-} and H_2CA were 2.607 Å for O4−H···O1 and 2.608 Å for O6−H···O2, which were shorter by about 0.08 Å than the typical distance of the O−H···O-type hydrogen bond.[37] Thus, this HBPT assembly **5** has three orthogonal hydrogen-bonded chains with relatively short hydrogen bonds, resulting in the formation of a 3-D rigid hydrogen-bonded network, as shown in Figure 6b. Solvated acetonitrile molecules formed no hydrogen bonds and were tightly packed in the 3-D hydrogen-bonded lattice.

Role of Solvent. As discussed above, we synthesized the 1-D, 2-D, and 3-D HBPT assemblies **3−5** in CH_3OH, THF, and CH_3CN solutions, respectively, despite the same D/A ratio (10:1). These interesting results suggest that the proton-donating/accepting ability of the solvent plays an important role in their crystal structures. In the case of assembly **3**, the CH_3OH was hydrogen-bonded to the CA^{2-} anion, leading to low dimensionality of the hydrogen-bonded network. The other solvent molecules formed no hydrogen bonds, and these solvent molecules were surrounded by the hydrogen-bonded framework. It is well known that CH_3OH can act as a weak proton donor in forming a hydrogen bond, whereas THF and CH_3CN are proton-accepting molecules. Thus, the dimensionality of the hydrogen-bonded network formed from $[Fe(Hpbph)_2]^{2+}$ and chloranilic acid would strongly depend on the proton-donating/accepting
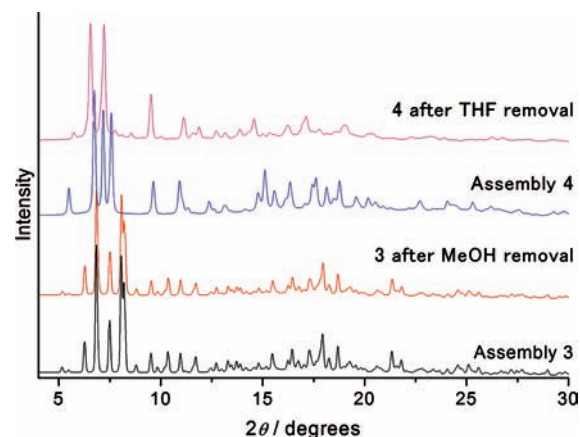
ability of the solvent. In addition, the polarity of the solvent would also contribute to determining their hydrogen-bonded network structures; that is, the protonation/deprotonation reactions would be suppressed in low-polar solvents, such as THF. In fact, the chloranilic acid molecules in the assembly **4** are not in the dianionic (CA^{2-}), but in the monoanionic (HCA^-) state. Thus, the difference in dimensionality of the hydrogen-bonded network between the assemblies **4** and **5** is probably due to the polarity of the solvent, which should strongly affect the pK_a values of proton-donating H_2CA and proton-accepting $[Fe(pbph)_2]$.

Thermal Stabilities of the HBPT Assemblies. To evaluate thermal stabilities, desorption temperatures of the solvents, and structural flexibilities of assemblies **3−5**, thermogravimetric analysis and powder X-ray diffraction (PXRD) were performed. Figure 7 shows the TG curves of assemblies **3**, **4**, and **5**. The TG curve of **3** indicates that a weight loss corresponding to the amount of two methanol molecules (5.9%) was observed up to 130 °C and then decomposed over 200 °C. In the TG curve of **4**, the weight loss observed up to 158 °C corresponds to the release of two THF molecules (10.5%). Over 220 °C, this assembly also decomposed. Unlike assemblies **3** and **4**, which showed evidence of the removal of lattice solvent molecules, assembly **5** did not exhibit weight loss corresponding to the release of two acetonitrile molecules up to the decomposition temperature of 120 °C. This is probably because those acetonitrile molecules are tightly packed by the robust network of hydrogen bonds among $[Fe(Hpbph)_2]^{2+}$, CA^{2-}, and H_2CA. Figure 8 shows the changes in the PXRD pattern of these assemblies. Observed diffraction patterns of assemblies **3** and **4** are identical to their patterns calculated from their crystal structures. After removal of the methanol of **3** by heating, the PXRD pattern was almost the same as that of the original **3**, suggesting that the crystal structure is sufficiently rigid to retain the structure without the solvated methanol molecules. This rigidity of the crystal is probably caused not by the hydrogen-bonded chain structure but by the tightly packed structure through van der Waals interactions. The PXRD pattern of HBPT assembly **5** also showed no change below the decomposition temperature (see Figure S1 in the Supporting Information). By contrast, the guest-free assembly **4** had a different pattern to that of the original THF-bound assembly, and the one-step change was observed in the temperature dependence of the PXRD pattern of the assembly **4** (see
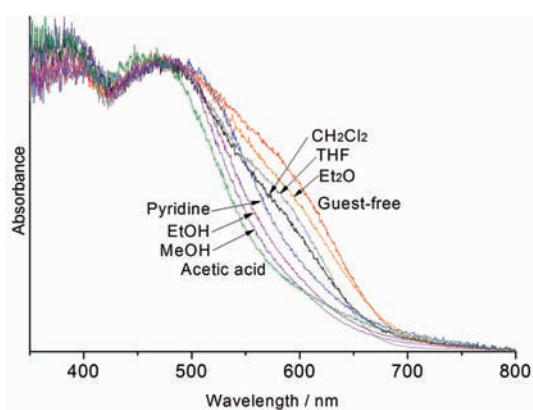
Figure 9. UV−vis diffuse reflectance spectral change in the guest-free assembly **4** under exposure to several organic vapors at room temperature.

Figure 10. Powder X-ray diffraction patterns of the guest-free assembly **4** before and after exposure to THF, CH_2Cl_2, CH_3OH, and acetic acid vapors at room temperature ($\lambda = 1.200(1)$ Å).

Figure S2 in the Supporting Information). After exposing the guest-free sample to THF vapor, the original pattern recovered. Thus, in the case of this assembly, reversible desorption and adsorption of THF vapor can occur, accompanied by structural transformation. These results suggest that the dimensionality of the hydrogen-bonded network affects the lattice rigidity and that the 2-D hydrogen-bonded network has moderate flexibility to exhibit vapochromic behavior.

Vapochromism Derived from the Rearrangement of the Hydrogen-Bonded Network. As mentioned in the Introduction, we have previously reported that the HBPT assembly composed of the planar-shaped Pd(II)−hydrazone complex and bromanilic acid shows unique vapochromic behavior in response to polar organic solvent vapors.[24] The result also suggests that the flexibility of the hydrogen-bonded network would play an important role in the vapochromism. As discussed above, because we have succeeded in controlling the dimensionality of the hydrogen-bonded network structure, we examined the vapochromic behavior of the assemblies **3**−**5** to evaluate the effect of the dimensionality of the hydrogen bond network structure on the vapochromic behavior. Assembly **4** exhibited vapochromic behavior in response to various organic vapors, including relatively low-polar solvent vapors, such as CH_2Cl_2 and chloroform, whereas the other two assemblies displayed no vapochromic behavior. Figure 9 shows the UV−vis diffuse reflectance spectral changes in assembly **4** under exposure to several organic vapors. The original THF-bound assembly **4** shows an intense absorption band at 480 nm with a shoulder at around 590 nm. After removal of the THF at 150 °C for 2 h, the absorption band at 480 nm did not change, but the shoulder at 590 nm became remarkably more intense. After exposing the no-vapor sample to THF vapor, the original absorption band was recovered. Thus, the color of this assembly **4** can be reversibly changed probably because of the release and adsorption of THF vapor. In addition, this assembly shows vapochromic behavior in response to the other organic vapors, as shown in Figure 9. The absorption intensity of the band shoulder moderately decreased under exposure to aprotic vapors, such as CH_2Cl_2, whereas it completely disappeared under exposure to protic vapors, such as acetic acid. These results suggest that this assembly shows vapochromic behavior in response to a variety of organic vapors. The HBPT assembly constructed of the Pd(II)−hydrazone complex and bromanilic acid exhibits vapochromic behavior
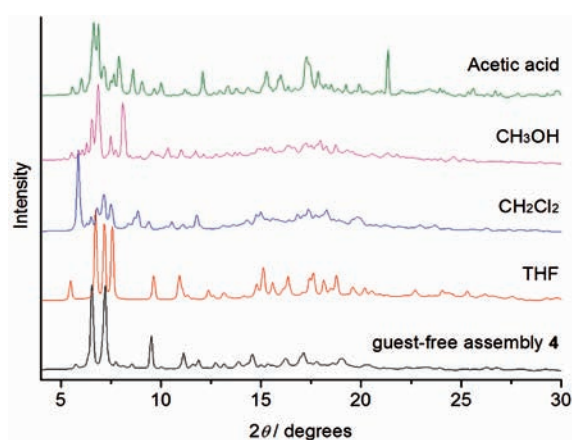
depending on the donor number of the vapor molecule. In contrast, the vapochromic behavior of the HBPT assembly **4** appears to be related to the protic/aprotic character of the vapor molecule. For example, the spectrum of **4** under exposure to CH_2Cl_2, which is a similar aprotic low-polar solvent to THF, resembled that of the THF-bound assembly. In contrast, the band shoulder at 613 nm completely disappeared in the spectra under exposure to highly polar protic vapors, such as CH_3OH and acetic acid, accompanied by a remarkable color change from brick-red to orange. Considering that the HCA^- anion showed a weak adsorption band at 525 nm in the solution state, and that the other HBPT assemblies **3** and **5** showed no adsorption band shoulder around 600 nm (see Figures S3 and S4 in the Supporting Information), the origin of this vapochromic behavior may be related to the deprotonation/protonation reaction and/or rearrangement of the hydrogen-bonded network around the HCA^- anion. To confirm whether the vapochromic behavior of this assembly originates from vapor-induced structural transformation, we examined PXRD patterns of the assemblies. Figure 10 shows changes in the PXRD pattern of **4** under exposure to several organic vapors. As mentioned above, the HBPT assembly **4** shows the reversible structural transformation induced by THF vapor adsorption/desorption. After exposure of the guest-free assembly to the other organic vapors, the obtained PXRD patterns differed from each other. These differences suggest that vapor-induced structural transformation of this assembly strongly depends on the organic vapor. Characteristic IR absorption bands of the adsorbed vapor molecules were observed in their spectra (see Figure S5 in the Supporting Information). In addition, thermogravimetric and elemental analyses of the samples after exposure of the guest-free assembly **4** to acetic acid, CH_2Cl_2, and CH_3OH vapors revealed that the guest-free assembly can absorb about 4 mol of acetic acid, 2 mol of CH_2Cl_2, and 2 mol of CH_3OH vapors, respectively (see Figure S6 and Table S1 in the Supporting Information). Except for the acetic acid-adsorbed sample, PXRD patterns were changed to the patterns identical to the guest-free assembly **4** by removal of these vapors (see Figure S7 in the Supporting Information). The PXRD pattern of the acetic acid-adsorbed assembly **4** was changed to an amorphous pattern by removal of acetic acid by heating it at 150 °C for 2 h. However, interestingly, upon exposure of these vapor-removed assemblies (even the amorphous solid

obtained from the removal of acetic acid) to THF vapor, all samples showed the patterns identical to that of the original THF-adsorbed assembly **4**. Thus, the guest-free assembly **4** can absorb these organic vapors to form the vapor-adsorbed phases formulated as $\{[Fe(Hpbph)_2](HCA)_2 \cdot 4CH_3COOH\}$, $\{[Fe(Hpbph)_2](HCA)_2 \cdot 2CH_2Cl_2\}$, and $\{[Fe(Hpbph)_2](HCA)_2 \cdot 2CH_3OH\}$, and release these vapors without any decomposition of the host HBPT framework or reaction between the host framework and guest molecules. We also confirmed that the direct guest exchange of the assembly **4** was achieved by exposure of the vapor-adsorbed assembly **4** to the other vapor (for example, the acetic acid-adsorbed assembly to THF-adsorbed assembly). Consequently, we conclude that the vapochromic behavior of HBPT assembly **4** originates from the structural transformation accompanied by vapor adsorption.

CONCLUSION

We synthesized protonated and deprotonated bis(hydrazone) iron(II) complexes, $[Fe(Hpbph)_2]Cl_2$ (**1**) and $[Fe(pbph)_2]$ (**2**), and determined the acid-dissociation constants to be 7.6 and 10.3. Taking advantage of the proton-accepting ability of the complex **2**, we synthesized three new HBPT assemblies, $\{[Fe(Hpbph)_2](CA) \cdot 2CH_3OH\}$ (**3**), $\{[Fe(Hpbph)_2](HCA)_2 \cdot 2THF\}$ (**4**), and $\{[Fe(Hpbph)_2](CA)(H_2CA)_2 \cdot 2CH_3CN\}$ (**5**), with different dimensionalities of the hydrogen-bonded network by the reaction of $[Fe(pbph)_2]$ with chloranilic acid (H_2CA) with a ratio of 1:10 in CH_3OH, THF, and CH_3CN, respectively. In the three HBPT assemblies, the bis(hydrazone)iron(II) complex molecule acted as a two-proton acceptor and adopted two protonated forms in all three HBPT assemblies. In contrast, the chloranilic acid acted as a proton donor and exhibited three different protonation states: neutral (**5**), monoanionic (**4**), and dianionic (**3** and **5**) states. In **3** and **5**, a 1-D hydrogen-bonded chain between CA^{2-} and $[Fe(Hpbph)_2]^{2+}$ was commonly formed, but the dimensionality of assembly **5** increased to three dimensions through the formation of two other hydrogen-bonded chains between H_2CA and CA^{2-}. In the HBPT assembly **4**, the 1-D hydrogen-bonded chains formed from only the HCA^- were connected by the $[Fe(Hpbph)_2]^{2+}$ cations to form a 2-D hydrogen-bonded sheet. Thermogravimetric analysis and PXRD measurements of these HBPT assemblies revealed that the dimensionality of the hydrogen-bonded network significantly contributes to the lattice rigidity and vapor adsorption properties. The 2-D HBPT assembly **4** shows interesting vapochromic behavior in response to a variety of organic solvent vapors. Further research focusing on the development of redox activity is now in progress.

ASSOCIATED CONTENT

S **Supporting Information.** X-ray crystallographic files of Hpbph ligand, Fe(II) complexes **1** and **2**, HBPT assemblies **3**, **4**, and **5** in CIF format; temperature dependence of PXRD pattern of **4** and **5**; UV–vis spectra of H_2CA, HCA^-, and CA^{2-} in methanol; UV–vis diffuse reflectance spectra of **3**, **4**, and **5**; IR spectral changes in assembly **4** under exposure to several organic vapors; TG curves and elemental analyses of assembly **4** obtained from the exposure of the guest-free assembly **4** to several organic vapors; and changes of PXRD patterns of CH_3OH, CH_2Cl_2 and acetic acid-adsorbed assembly **4**. This material is available free of charge via the Internet at http://pubs.acs.org.

AUTHOR INFORMATION

Corresponding Author

*E-mail: akoba@sci.hokudai.ac.jp (A.K.), mkato@sci.hokudai.ac.jp (M.K.). Phone: +81-11-706-3819 (A.K.), +81-11-706-3817 (M.K.). Fax: +81-11-706-3447 (A.K.), +81-11-706-3447 (M.K.).

REFERENCES

(1) Daws, C. A.; Exstrom, C. L.; Sowa, J. R., Jr.; Mann, K. R. *Chem. Mater.* **1997**, *9*, 363–368.

(2) Kunugi, Y.; Miller, L. L.; Mann, K. R.; Pomije, M. K. *Chem. Mater.* **1998**, *10*, 1487–1489.

(3) Kunugi, Y.; Mann, K. R.; Miller, L. L.; Exstrom, C. L. *J. Am. Chem. Soc.* **1998**, *120*, 589–590.

(4) Beauvais, L. G.; Shores, M. P.; Long, J. R. *J. Am. Chem. Soc.* **2000**, *122*, 2763–2772.

(5) Albrecht, M.; Lutz, M.; Spek, A. L.; Van, Koten, G. *Nature* **2000**, *406*, 970–974.

(6) Fernández, E. J.; López-de-Luzuriaga, J. M.; Monge, M.; Olmos, M. E.; Pérez, J.; Laguna, A.; Mohamed, A. A.; Fackler., J. P. *J. Am. Chem. Soc.* **2003**, *125*, 2022–2023.

(7) McGee, K. A.; Marquardt, B. J.; Mann, K. R. *Inorg. Chem.* **2008**, *47*, 9143–9145.

(8) Katz, M. J.; Ramnial, T.; Yu, H. Z.; Leznoff, D. B. *J. Am. Chem. Soc.* **2008**, *130*, 10662–10673.

(9) Cicha, M. J.; Hill, I. M.; Lackner, A. D.; Martineza, R. J.; Ruthenburga, T. C.; Takeshitaa, Y.; Younga, A. J.; Drewa, S. M.; Bussb, C. E.; Mannb, K. R. *Sens. Actuators, B* **2010**, *149*, 199–204.

(10) Abe, T.; Suzuki, T.; Shinozaki, K. *Inorg. Chem.* **2010**, *49*, 1794–1800.

(11) (a) Kato, M.; Omura, A.; Toshikawa, A.; Kishi, S.; Sugimoto, Y. *Angew. Chem., Int. Ed.* **2002**, *41*, 3183–3185. (b) Grove, L. J.; Rennekamp, J. M.; Jude, H.; Connick, W. B. *J. Am. Chem. Soc.* **2004**, *126*, 1594–1595. (c) Kato, M.; Kishi, S.; Wakamatsu, Y.; Sugi, Y.; Osamura, Y.; Koshiyama, T.; Hasegawa, M. *Chem. Lett.* **2005**, *34*, 1368–1369. (d) Drew, S. M.; Smith, L. I.; McGee, K. A.; Mann, K. R. *Chem. Mater.* **2009**, *21*, 3117–3124.

(12) (a) Wadas, T. J.; Wang, Q.-M.; Kin, Y.-J.; Flaschenreim, C.; Blanton, T. N.; Eisenberg, R. *J. Am. Chem. Soc.* **2004**, *126*, 16841–16849. (b) Grove, L. J.; Oliver, A. G.; Krause, J. A.; Connick, W. B. *Inorg. Chem.* **2008**, *47*, 1408–1410. (c) Du, P.; Schineider, J.; Brennessel, W. W.; Eisenberg, R. *Inorg. Chem.* **2008**, *47*, 69–77.

(13) (a) Vickery, J. C.; Olmstead, M. M.; Fung, E. Y.; Balch, A. L. *Angew. Chem., Int. Ed. Engl.* **1997**, *36*, 1179–1181. (b) Mansour, M. A.; Connick, W. B.; lachicotte, R. J.; Gysling, H. J.; Eisenberg, R. *J. Am. Chem. Soc.* **1998**, *120*, 1329–1330. (c) Rawashdeh-Omary, M. A.; Omary, M. A.; Fackler, J. P., Jr. *J. Am. Chem. Soc.* **2001**, *123*, 9689–9691.

(14) Fernández, E. J.; López-de-Luzuriaga, J. M.; Monge, M.; Olmos, M. E.; Puelles, R. C.; Laguna, A.; Mohamed, A. A.; Fackler, J. P. *Inorg. Chem.* **2008**, *47*, 8069–8076.

(15) Strasser, C. E.; Catalano, V. J. *J. Am. Chem. Soc.* **2010**, *132*, 10009–10011.

(16) (a) Fernández, E. J.; López-de-Luzuriaga, J. M.; Monge, M.; Montiel, M.; Olmos, M. E.; P Pérez, J.; Laguna, A.; Mendizábal, F.; Mohamed, A. A.; Fackler, J. P. *Inorg. Chem.* **2004**, *44*, 3573–3581. (b) Lefebvre, J.; Batchelor, R. J.; Leznoff, D. B. *J. Am. Chem. Soc.* **2004**, *126*, 16117–16125. (c) Yamada, K.; Tanaka, H.; Yagishita, S.; Adachi, K.;

8316

dx.doi.org/10.1021/ic2008396 |*Inorg. Chem.* 2011, 50, 8308–8317

Uenura, T.; Kitagawa, S.; Kawata, S. *Inorg. Chem.* **2006**, *45*, 4322–4324. (d) Bencini, A.; Casarin, M.; Forrer, D.; Franco, L.; Garau, F.; Masciocchi, N.; Pandalfo, L.; Pettinari, C.; Ruzzi, M.; Vittadini, A. *Inorg. Chem.* **2009**, *48*, 4044–4051.

(17) (a) Yamada, K.; Yagishita, S.; Tanaka, H.; Tohyama, K.; Adachi, K.; Kaizaki, S.; Kumagai, H.; Inoue, K.; Kitaura, R.; Chang, H.-C.; Kitagawa, S.; Kawata, S. *Chem.—Eur. J.* **2004**, *10*, 2647–2660. (b) Takahashi, E.; Takaya, H.; Naota, T. *Chem.—Eur. J.* **2010**, *16*, 4793–4802.

(18) (a) Lu, W.; Chan, M. C. W.; Cheung, K.-K.; Che, C.-M. *Organometallics* **2001**, *20*, 2477–2486. (b) Lu, W.; Chang, M. C. W.; Zhu, N.; Che, C.-M.; He, Z.; Wong, K.-Y. *Chem.—Eur. J.* **2003**, *9*, 6155–6166. (c) Liu, Z.; Bian, Z.; Bian, J.; Li, Z.; Nie, D.; Huang, C. *Inorg. Chem.* **2008**, *47*, 8025–8030.

(19) (a) Shibuya, Y.; Nabari, K.; Kondo, M.; Yasue, S.; Maeda, K.; Uchida, F.; Kawaguchi, H. *Chem. Lett.* **2008**, *37*, 78–79. (b) Mobin, S. M.; Srivastava, A. K.; Marthur, P.; Lahiri, G. K. *Dalton Trans.* **2010**, *39*, 1447–1449.

(20) (a) Kreuer, K. D. *Chem. Mater.* **1996**, *8*, 610–641. (b) Zhang, B.; Cai, Y.; Mu, X.; Lou, N.; Wang, X. *Chem. Phys. Lett.* **2002**, *351*, 335–340. (c) Wilson, C. C.; Goeta, A. E. *Angew. Chem., Int. Ed.* **2004**, *43*, 2095–2099. (d) Agmon, N. *J. Phys. Chem.* **2005**, *109*, 12–35. (e) Martins, D. M. S.; Middlemiss, D. S.; Pulham, C. R.; Wilson, C. C.; Weller, M. T.; Henry, P. F.; Shankland, M.; Shankland, K.; Marshall, W. G.; Ibberson, R. M.; Knight, K.; Moggach, S.; Brunelli, M.; Morrison, C. A. *J. Am. Chem. Soc.* **2009**, *131*, 3884–3893.

(21) (a) Burrows, A. D.; Harrington, R. W.; Mahon, M. F.; Price, C. E. *J. Chem. Soc., Dalton Trans.* **2000**, *21*, 3845–3854. (b) Zaman, M. B.; Tomura, M.; Yamashita, Y. *J. Org. Chem.* **2001**, *66*, 5987–5995. (c) Kobayashi, K.; Sato, A.; Sakamoto, S.; Yamaguchi, K. *J. Am. Chem. Soc.* **2003**, *125*, 3035–3045. (d) Du, M.; Zhang, Z.-H.; Zhao, X.-J. *Cryst. Growth Des.* **2005**, *5*, 1199–1208. (e) Murata, T.; Morita, Y.; Yakiyama, Y.; Fukui, K.; Yamochi, H.; Saito, G.; Nakasuji, K. *J. Am. Chem. Soc.* **2007**, *129*, 10837–10846.

(22) (a) Zaman, Md. B.; Morita, Y.; Toyoda, J.; Yamochi, H.; Saito, G.; Yoneyama, N.; Enoki, T.; Nakasuji, K. *Chem. Lett.* **1997**, *26*, 729–730. (b) Zaman, Md. B.; Tomura, M.; Yamashita, Y. *J. Org. Chem.* **2001**, *66*, 5987–5995. (c) Kabir, M. K.; Tobita, H.; Matsuo, H.; Nagayoshi, K.; Yamada, K.; Adachi, K.; Sugiyama, Y.; Kitagawa, S.; Kawata, S. *Cryst. Growth Des.* **2003**, *3*, 791–798. (d) Gotoh, K.; Asaji, T.; Ishida, H. *Acta Crystallogr., Sect. C* **2007**, *63*, o17–o20. (e) Horiuchi, S.; Kumai, R.; Tokunaga, Y.; Tokura, Y. *J. Am. Chem. Soc.* **2008**, *130*, 13382–13391. (f) Gotoh, K.; Nagoshi, H.; Ishida, H. *Acta Crystallogr., Sect. C* **2009**, *65*, o273–o277. (g) Horiuchi, S.; Kumai, R.; Tokura, Y. *J. Mater. Chem.* **2009**, *19*, 4421–4434.

(23) (a) Elsayed, M. A.; Agarwal, S. *Talanta* **1982**, *29*, 535–537. (b) Gohar, G. A.; Habeeb, M. M. *Spectroscopy* **2000**, *14*, 99–107.

(24) Yamada, K.; Yagishita, S.; Tanaka, H.; Tohyama, K.; Adachi, K.; Kaizaki, S.; Kumagai, H.; Inoue, K.; Kitaura, R.; Chang, H.-C.; Kitagawa, S.; Kawata, S. *Chem.—Eur. J.* **2004**, *10*, 2647–2660.

(25) Chang, M.; Horiki, H.; Nakajima, K.; Kobayashi, A.; Chang, H.-C.; Kato, M. *Bull. Chem. Soc. Jpn.* **2010**, *83*, 905–910.

(26) Kobayashi, A.; Dosen, M.-A.; Chang, M.; Nakajima, K.; Noro, S.-I.; Kato, M. *J. Am. Chem. Soc.* **2010**, *132*, 15286–15298.

(27) Bacchi, A.; Carcelli, M.; Costa, M.; Fochi, A.; Monici, C.; Pelagatti, P.; Pelizzi, C.; Pelizzi, G.; Roca, L. M. S. *J. Organomet. Chem.* **2000**, *593—594*, 180–191.

(28) *CrystalClear*; Molecular Structure Corporation: Orem, UT, 2001.

(29) SIR-92: Altomare, A.; Cascarano, G.; Giacovazzo, C.; Guagliardi, A.; Burla, M.; Polidori, G.; Camalli, M. *J. Appl. Crystallogr.* **1994**, *27*, 435–436.

(30) Sheldrick, G. M. *SHLEX*-97; University of Göttingen: Göttingen, Germany, 1997.

(31) Hutchinson, D. J.; Hanton, L. R.; Moratti, S. C. *Inorg. Chem.* **2010**, *49*, 5923–5934.

(32) Basu, C.; Chowdhury, S.; Banerjee, R.; Evans, H. S.; Mukherjee, S. *Polyhedron* **2007**, *26*, 3617–3624.

(33) (a) Kohata, K.; Kawamonzen, Y.; Odashima, T.; Ishii, H. *Bull. Chem. Soc. Jpn.* **1990**, *63*, 3398–3404. (b) Lu, Y.-H.; Lu, Y.-W.; Wu, C.-L.; Shao, Q.; Chen, X.-L.; Bimbong, R. N. B. *Spectrochim. Acta, Part A* **2006**, *65*, 695–701.

(34) Andersen, E. K. *Acta Crystallogr.* **1967**, *22*, 188–191.

(35) (a) Ishida, H.; Kashino, S. *Acta Crystallogr., Sect. C* **1999**, *55*, 1149–1152. (b) Ishida, H.; Kashino, S. *Acta Crystallogr., Sect. C* **2001**, *57*, 476–479.

(36) Andersen, E. K. *Acta Crystallogr.* **1967**, *2*, 196–201.

(37) Akhtaruzzaman, M. D.; Tomura, M.; Takahashi, K.; Nishida, J.-I.; Yamashita, Y. *Supramol. Chem.* **2003**, *15*, 239–243.

8317

dx.doi.org/10.1021/ic2008396 |*Inorg. Chem.* 2011, 50, 8308–8317